

## Efficient purification of oily wastewater by a single-stage filtration with diatomite/carbon membranes

Yonghong Wu<sup>a</sup>, Rui Yao<sup>a</sup>, Xueqian Hong<sup>a</sup>, Bing Zhang<sup>a,\*</sup>, Tonghua Wang<sup>b</sup>

<sup>a</sup>School of Petrochemical Engineering, Shenyang University of Technology, No. 30, Guanghua Street, Hongwei District, Liaoyang 111003, China, emails: bzhangdut@163.com/zhangbing@sut.edu.cn (B. Zhang), wuyh@sut.edu.cn (Y. Wu), yaoruirrr@163.com (R. Yao), xqhong301@163.com (X. Hong)

<sup>b</sup>Carbon Research Laboratory, State Key Lab of Fine Chemicals, School of Chemical Engineering, Dalian University of Technology, No. 2, Linggong Road, Dalian 116024, China, email: wangth@dlut.edu.cn

Received 13 September 2020; Accepted 12 May 2021

---

### ABSTRACT

In this work, a single-stage filtration was developed for the first time as an effective protocol for the purification of oily wastewater via diatomite/carbon composite microfiltration membranes. The microstructure and property of microfiltration carbon membranes (MFCMs) were modulated by varying the diatomites dosage for purifying oily wastewater with single-stage filtration. Results demonstrated that the diatomite addition was favorable for the thermal stability of precursors and the structural compactness of resultant MFCMs. The maximum oil rejection can reach 98.9%, along with the permeation flux of 147.86 kg m<sup>-2</sup> h<sup>-1</sup> by a single-stage filtration of MFCMs. In addition, the adoption of post-oxidation can further greatly improve the permeation flux and antifouling ability of MFCMs for oily wastewater.

*Keywords:* Oil–water separation; Microfiltration; Carbon membranes; Diatomite

---

### 1. Introduction

The excessive exploitation and indulgent consumption of fossil fuel have incurred revenge on human beings by the punishment from nature, such as depletion of nonrenewable resources, deterioration of environmental contamination, and so forth [1]. People are more aware of the importance of protecting the natural environment by various advanced technologies. One concern is the treatment of a large amount of by-produced oily wastewater discharged from many sections of daily life and industrial production [2–4]. So far, some traditional technologies, including flocculation, air flotation, gravity separation, etc., can be applied for the treatment of oily wastewater [5–7]. However, most of them are subjected to the disadvantages of high operation cost, low

efficiency, especially for the invalid mitigation of emulsified oil in wastewater [8,9]. As such, it is necessary to develop more feasible and efficient technology.

Recently, membrane-based separation technologies, that is, microfiltration [10], ultrafiltration [11], nanofiltration [12], reverse osmosis [13], have been verified to be useful for the purification of oily wastewater. Nevertheless, the existing polymeric membranes are frequently suffered from the issue of severe membrane fouling as the result of surfactant adsorption, pore plugging by oil droplets, as well as textural degradation [14,15]. Differently, microfiltration carbon membranes (MFCMs) have been identified as a promising candidate for the treatment of oily

---

\* Corresponding author.

effluents by virtue of high efficiency, chemical inertness, mechanically robustness, etc. [16,17]. Li et al. [18] studied the oil separation efficiency by coal-based MFCMs coupled with an electric field, of which the oil rejection was above 95%. Meanwhile, they also found that the combination of an electric field and acidic conditions can significantly improve the antifouling ability of MFCMs. Pan et al. [19] also applied coal-based MFCMs to separate oil-in-water emulsion and gained an oil rejection of over 98%. Wu et al. [16] prepared phenolic resin-based MFCMs for oily wastewater treatment and achieved an optimum oil rejection of 95.3%. Moreover, we also found that the presence of ethanol as a demulsifier is more beneficial for the MFCMs to purify oil-in-water. Song et al. [17] investigated the effect of carbonization conditions on the structure and separation property of MFCMs. Du et al. [20] effectively increased the separation efficiency up to 99.5% for oil-water emulsion by modifying the surface wettability of MFCMs. El-Sayed et al. [21] removed oil from the water depending on the dynamic adsorption capacity of amorphous carbon thin film packed in a column bed. Derbel and Amar [22] prepared tubular ultrafiltration/microfiltration composite carbon membranes for the application of air gap membrane distillation of oily wastewater treatment, of which the oil retention was up to 99%.

Previously, we developed a type of diatomite hybrid MFCMs that exhibited a most satisfactory oil rejection of 97.8% for oily wastewater [23]. Furthermore, the oil rejection of MFCMs was positively related to the amount of diatomite in the membrane matrix. Nevertheless, several issues are still remained to be tackled for the MFCMs prior to practical application. The first one is the pretreatment of MFCMs by water rinsing before wastewater treatment for the sake of rapidly reaching a steady filtration state. That additional step is definitely time-consuming and laborious in operation. In addition, it is also significant to modify the surface wettability of MFCMs in order to further increase the anti-fouling ability and the purified water production. In this regard, here the strategies of single-stage filtration and post-oxidation modification were attempted to overcome the above-mentioned two issues of MFCMs.

## 2. Experimental

### 2.1. Raw materials

Diatomite (technical grade) with a particulate size of 20–40  $\mu\text{m}$  was acquired from Beichen Fangzheng Reagent Factory in Tianjin of China, without further treatment. Phenolic resin (technical grade, Xinxiang Boma Fengfan Industrial Co., Ltd.), hexamethylenetetramine (analytical grade) and sodium carboxymethyl cellulose (technical grade) were commercially procured from Sinopharm Chemical Reagent Co., Ltd. of China. The crude oil was produced from Turmin Oil Field in Russia. Homemade double-distilled water was utilized to prepare oily wastewater in this study.

### 2.2. Preparation of MFCMs

First, a powder mixture of phenolic resin and hexamethylenetetramine in a mass ratio of 25:3 was formed by

mechanically blending and grinding. After that, the mixture was partly cured at 150°C for 1 h. Then, the yielded spongy-like product was pulverized to the particle diameter beneath 100  $\mu\text{m}$  before use. Next, sodium carboxymethyl cellulose and diatomite were continuously added to form a starting mixture with the corresponding mass fractions of 20 wt.% and 15–35 wt.%, respectively. Subsequently, a plasticine-like paste was obtained with the aid of the proper amount of water, manual kneading and aging for 80 min. Finally, the precursor membranes with a diameter of 3 cm and thickness of 5 mm were shaped from the paste in a molding machine operated at 4 MPa, after drying for 10–15 d at room temperature. The code PM- $t\%$  was labeled for the precursor membranes, referring to the diatomite content of  $t$  wt.% in the starting mixture.

The carbonization of precursor membranes was conducted in a horizontal furnace under a flowing nitrogen atmosphere of 100 mL  $\text{min}^{-1}$  as per the temperature history in Fig. 1. Finally, MFCMs were obtained after natural cooling down to room temperature. The MFCMs made from PM- $t\%$  were labeled with CM- $t\%$ . Fig. 2 is the photographs of precursor membranes and derived MFCMs.

In addition, post-oxidation was utilized to improve the anti-fouling ability of MFCMs. The MFCMs were annealed at 200°C for 30 min at a heating rate of 2°C  $\text{min}^{-1}$  from ambient temperature under flowing air of 100 mL  $\text{min}^{-1}$ . The treated MFCMs were marked as PO-CM- $t\%$ .

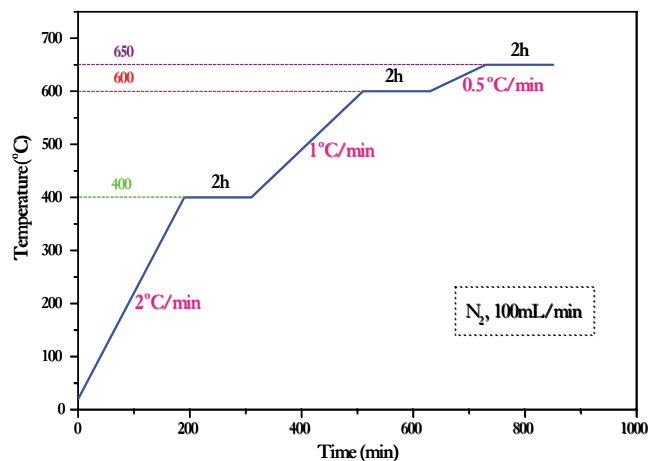


Fig. 1. The heating program of carbonization for the preparation of MFCMs.

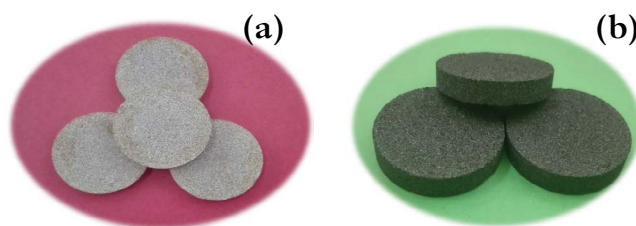


Fig. 2. Photographs of membrane samples: (a) precursor membranes and (b) MFCMs.

2.3. Characterization methods

The thermal stability of precursor membranes was tested by a TGA 4000 thermogravimetric analyzer (Perkin Elmer, USA) in a temperature range of ambient temperature to 800°C at 20°C min<sup>-1</sup> and flowing nitrogen of 20 mL min<sup>-1</sup>.

The surface functional groups of membranes were detected by a TENSOR II Platinum ATR-FTIR (Bruker), in the wavenumber range of 4,000–400 cm<sup>-1</sup> at a resolution of 0.5 cm<sup>-1</sup> with averaging 15 scanning times.

The morphology of MFCMs was observed by a TM-3000 scanning electron microscope (Hitachi) at standard mode and accelerating voltage of 15 kV.

The microstructure of samples was analyzed using an Ultima IV X-ray diffractometer (Rigaku) at an accelerating voltage of 40 kV, a current of 40 mA and a scanning speed of 10°C min<sup>-1</sup>. The interlayer distance ( $d_{002}$  values) were also calculated by Bragg’s formula Eq. (1):

$$d_{002} = \frac{\lambda}{(2\sin\theta)} \tag{1}$$

where  $\lambda$  and  $\theta$  are the diffraction wavelength (0.15405 nm) and diffraction angle, respectively.

The porosity of MFCMs was measured by a standard boiling method in GB/T1966-1996, [24] with Eq. (2).

$$q = \frac{m_2 - m_1}{m_2 - m_3} \times 100\% \tag{2}$$

where  $m_1$ ,  $m_2$  and  $m_3$  are the dry weight (g), wet weight (g) and saturated weight (g) of MFCMs, respectively.

The pore size distribution of MFCMs was determined by a popular bubble-pressure method [25].

The surface wettability of membranes in the air was evaluated by the water contact angles that were calculated by a series of dynamic photos successively taken by a JC2000D contact angle analyzer. During the test process, 10  $\mu$ L distilled water was dropped on the dried membrane sample placed on a horizontal glass slide.

The adsorption test of MFCMs was performed using a SHA-C constant-temperature shaker at 30°C  $\pm$  1°C and 100 rpm min<sup>-1</sup>, where the MFCMs were ground into powder as adsorbent.

2.4. Purification of oily wastewater

First of all, emulsified oily wastewater was prepared by adding the proper amount of crude oil into double-distilled water under vigorously mechanical and ultrasonic agitation for 2 h. Then, a standardized equation on the relationship between oil concentration and absorbance was regressed by measuring the standard solutions with a UV1800 PC UV-visible spectrophotometer at a wavelength of 222 nm.

The purification of oily wastewater was conducted by a single-stage filtration of MFCMs with the experimental setup in Fig. 3. Initially, the feed flux was set at 40 mL min<sup>-1</sup> by a piston pump with the release valve fully shutting down. When penetrating fluid was received the downstream of membrane cell, the feed flux was promptly regulated to the required value at a trans-membrane pressure of 0.02 MPa. After filtration, the feed pipeline was switched to a washing line with 30 mL min<sup>-1</sup> of double-distilled fresh water for 20 min.

The permeation flux ( $J$ ) of MFCMs was calculated by Eq. (3):

$$J = \frac{W \times 600}{t \times S} \tag{3}$$

where  $W$ ,  $t$  and  $S$  were the collected weight of penetrating fluid (g), running time (min) and effective area (cm<sup>2</sup>), respectively.

The oil rejection ( $R$ ) was obtained according to Eq. (4):

$$R(\%) = \left(1 - \frac{C_p}{C_f}\right) \times 100\% \tag{4}$$

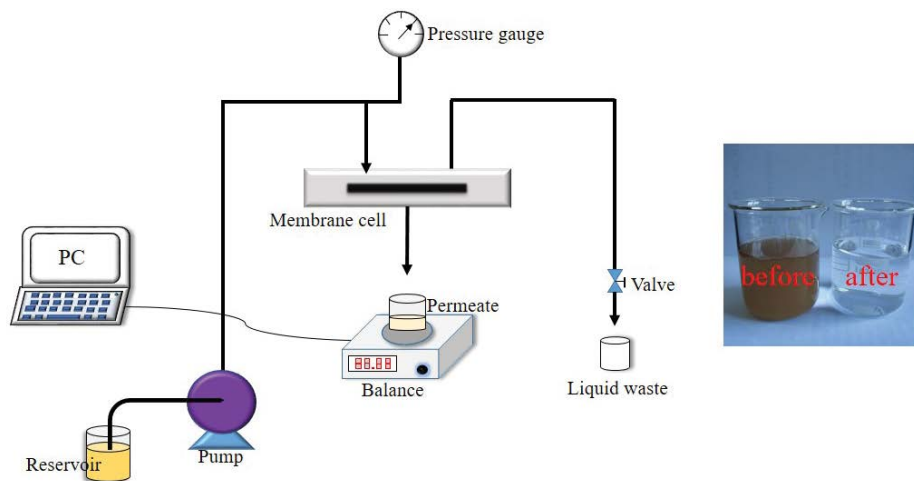


Fig. 3. Schematic of the experimental setup for oily wastewater treatment by single-stage.

where  $C_p$  and  $C_f$  were the oil concentrations ( $\text{mg L}^{-1}$ ) at the permeate stream and feed stream, respectively.

### 3. Results and discussion

#### 3.1. Thermogravimetric analysis of precursor membranes

Fig. 4 shows that diatomite has excellent thermal stability with near-zero weight loss throughout the whole pyrolysis process. In contrast, precursor membranes undergo three major degradation stages during pyrolysis. The first one locates at  $30^\circ\text{C}$ – $170^\circ\text{C}$  due to the removal of physically adsorbed water and chemically derived gases by further curing of phenolic resin. The second one occurs at  $170^\circ\text{C}$ – $350^\circ\text{C}$  due to the thermal degradation of sodium carboxymethyl cellulose. The third stage is in the range of  $350^\circ\text{C}$ – $650^\circ\text{C}$  due to the thermal decomposition of the molecular main chain of phenolic resin, resulting in the evolution of a large amount of various gases and volatiles, for instance,  $\text{CO}_2$ ,  $\text{CH}_4$  and so on [26]. The profile of weight loss curves gradually turns to be flat after  $650^\circ\text{C}$ , indicating that the thermal decomposition reaction is approaching the termination point. Therefore, the adoption of carbonization temperature at  $650^\circ\text{C}$  in this work could guarantee the full development of pores in MFCMs. Moreover, in comparison to PM-0%, the thermal stability is considerably enhanced with increasing the diatomite amount in the precursor. Probably, the embedded diatomite particles interact with the molecular chains of phenolic resin via their surface silanol groups since the bonding energy of Si–O ( $423 \text{ kJ mol}^{-1}$ ) is much higher than C–O ( $384 \text{ kJ mol}^{-1}$ ) and C–C bonds. Thus, it is helpful for improving the thermal weight remaining of precursor membranes [25].

#### 3.2. Functional groups

Fig. 5 is the Fourier-transform infrared spectroscopy (FTIR) of membrane samples. By comparison, it is clearly found that the characteristic peaks of Si–O–Si bond stretching for diatomite appear in hybrid precursor membranes at  $1,073$ ,  $791$  and  $466 \text{ cm}^{-1}$  [27]. Besides, some other peaks are assigned to benzene at  $1,596 \text{ cm}^{-1}$ , C=C bond

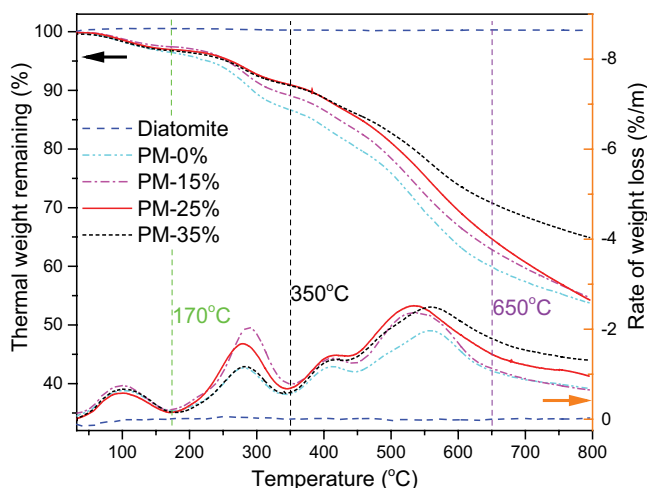


Fig. 4. Thermal weight loss curves of precursor membranes.

stretching model of aromatic hydrocarbon and benzene rings at  $1,501 \text{ cm}^{-1}$ . Moreover, the peak intensity of  $1,231$  and  $1,003 \text{ cm}^{-1}$  is obviously reduced for the precursor membranes after introducing diatomite, along with the appearance of some new peaks at  $1,073$ ,  $791$ ,  $616$  and  $466 \text{ cm}^{-1}$  [28]. This phenomenon confirms the foregoing deduction in TGA section. Namely, the diatomite interacts with phenolic resin through their electronegativity and –OH bond in phenolic resin in form of hydrogen bonding [25].

Fig. 5b indicates that the characteristic peak of Si–O–Si of diatomite remains in MFCMs. This proves that the microstructure of diatomite is properly preserved in the membrane matrix after carbonization. Differently, most of the functional groups of the phenolic resin have been depleted from the molecular chains after carbonization. The result is in good agreement with the previous thermogravimetry analysis.

#### 3.3. Morphology observation

Fig. 6 presents the scanning electron microscopy (SEM) images of samples. Clearly, the pristine diatomite is in the

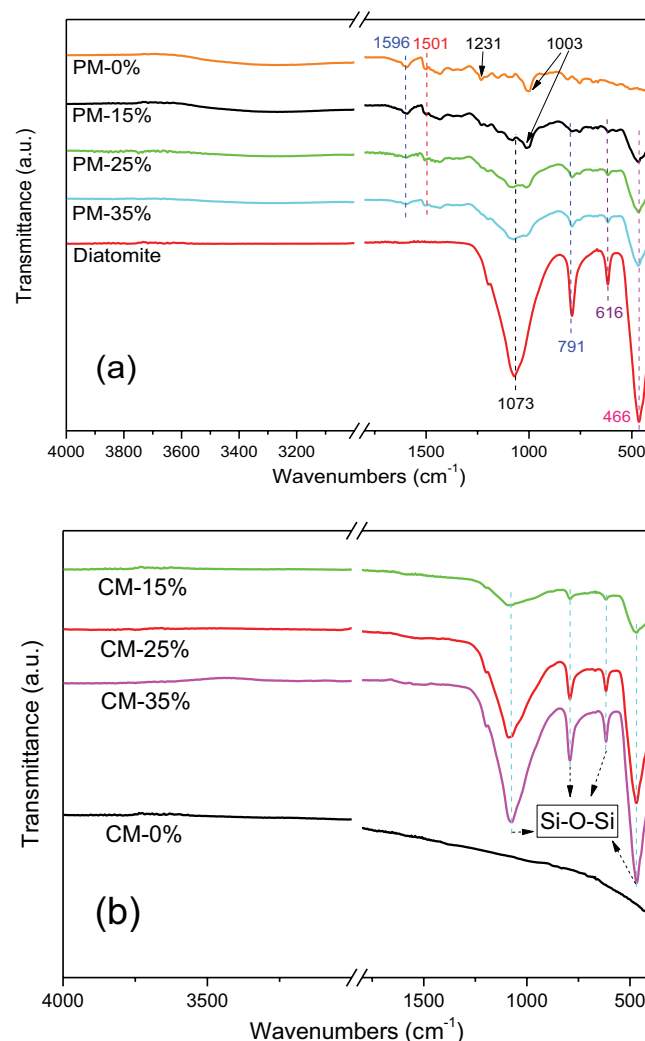


Fig. 5. FTIR spectra of (a) precursor membranes and (b) MFCMs.

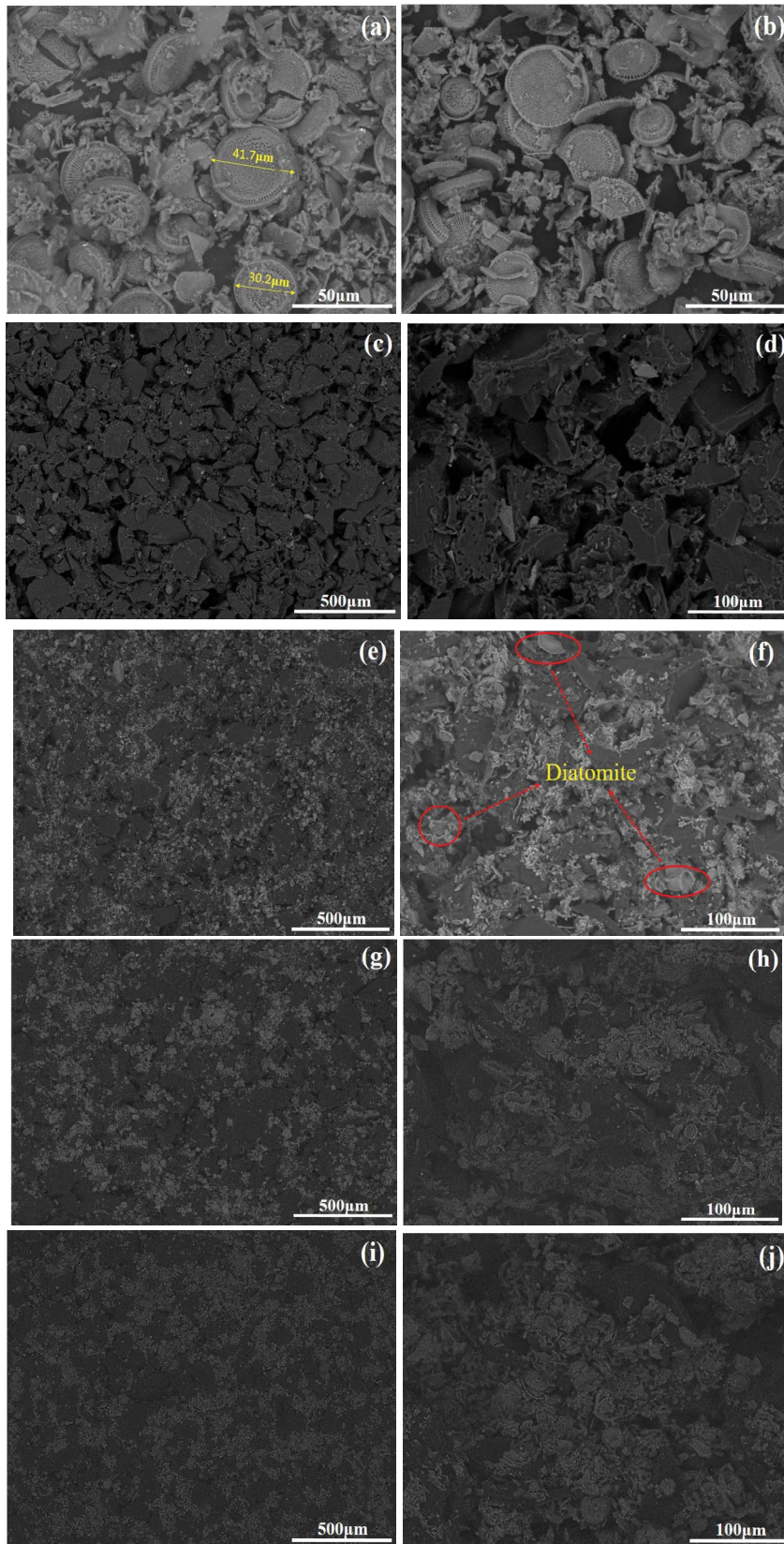


Fig. 6. SEM images of diatomite hybrid MFCMs. (a,b) Diatomite before and after carbonization, (c,d) surface and cross-section of CM-0%, (e,f) CM-15%, (g,h) CM-25%, and (i,j) CM-35%.

form of a circular disk of 30–40  $\mu\text{m}$  in diameter with regularly arranged holes of 300–500 nm opening width. This agrees well with the literature [29]. The apparent shape of diatomite remains well after carbonization at elevated temperature, which verifies the previous TGA and FTIR results. For MFCMs, the quantity of embedded white dots representing diatomite increases in SEM images as the diatomite amount increases. It means that carbonization does not destroy the porous structure and surface nature of diatomite [30].

The SEM images also show that the porous structure of CM-0% is mainly composed of the chaotic stacking of carbon lumps or pieces, of which the porous texture is significantly different in shapes and sizes. In particular, with the variation of diatomite amount, the quantity and dimension of macropores are substantially changed in MFCMs. The reason lies in the fact that the diatomites can not only influence the stacking style of carbon substrates but also create additional interfacial pores in MFCMs. In this way, the diatomites take a great effect on the porous structure and the separation performance of final MFCMs.

### 3.4. Microstructure analysis

In the X-ray diffraction (XRD) patterns (Fig. 7), the typical diffraction peaks of diatomites could be clearly identified in MFCMs at  $21.7^\circ$ ,  $28.1^\circ$ ,  $31.1^\circ$  and  $35.8^\circ$ , representing amorphous  $\text{SiO}_2$ ,  $\text{Al}_2\text{O}_3$  and  $\text{CaO}$ , respectively [27]. Moreover, the peak intensities are dramatically enhanced with the increase of the diatomite amount. It suggests that the microstructure of diatomite is intact in the membrane matrix even though after carbonization, which is consistent with the results of TGA and FTIR analysis.

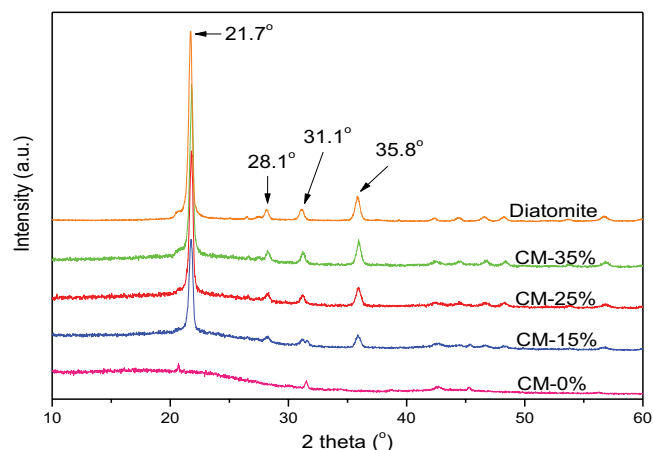


Fig. 7. XRD patterns of MFCMs with varying diatomite amount.

Table 1  
Structural parameters and surface wettability of MFCMs blended with diatomite

Membrane samples	$d_{002}$ values (nm)	Mean pore size ( $\mu\text{m}$ )	Porosity (%)	Water contact angles ( $^\circ$ )
CM-0%	0.5043	0.85	52.63	74
CM-15%	0.4126	0.39	53.21	103
CM-25%	0.4096	0.37	52.64	99
CM-35%	0.4070	0.51	53.56	107

Table 1 lists the  $d_{002}$  values of MFCMs, which are frequently referred to the distance between the crystalline planes of the amorphous carbon matrix. It shows that the  $d_{002}$  values gradually decrease from 0.5043 nm to 0.4070 nm as the amount of diatomite increases. This change tendency of microstructural compactness will be further discussed in the following porous structure analysis.

### 3.5. Porous structure analysis

Table 1 also gives the porous parameters of as-prepared MFCMs. As the amount of diatomite increases from 0 to 25 wt.%, the mean pore size of MFCMs decreases from 0.85 to 0.37  $\mu\text{m}$ . Then, it increases again to 0.51  $\mu\text{m}$  when the amount is further increased to 35%. In the case of porosity, the change is not apparent within the scope of  $53.0\% \pm 0.5\%$ .

When the content of diatomite is relatively low, it is beneficial for their uniform dispersion in starting materials so as to constitute a narrow pore size distribution in MFCMs (Fig. 8). Meanwhile, the pore size tends to be reduced as the result of more diatomite particles filling into the larger pores performed by carbon fragments stacking in MFCMs. This result agrees well with the previous XRD analysis and SEM observation. It is attributed to the pore blockage by the accumulation of compact framework of diatomites in the matrix. In addition, a large amount of diatomite might also retard the thermal curing reaction of phenolic resin during the early stage of carbonization, leading to the derivation of a more dense structure with a higher graphitization degree in the final carbon matrix. However, the change tendency of the mean pore size of MFCMs turns to

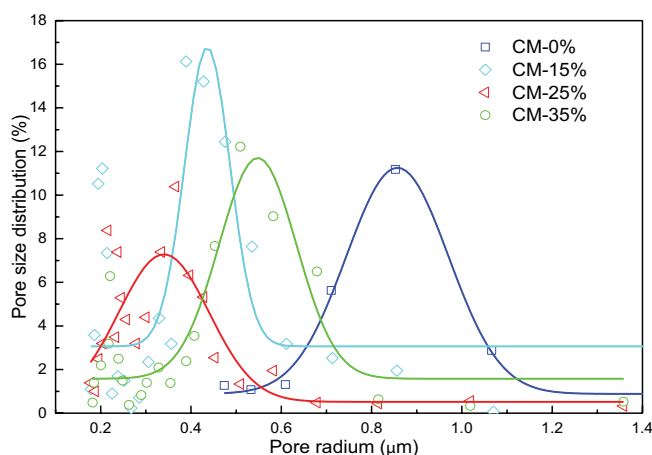


Fig. 8. Pore size distributions of MFCMs with varying diatomite amount.

the opposite direction when the amount of diatomite is elevated to an extremely high value (e.g., 35%). The formation of larger pores is ascribed to the disorderly accumulation of a large amount of diatomites without the decoration of carbon pieces [30]. Simultaneously, the mechanical strength of MFCMs would also be remarkably decreased in such circumstances of less tight adherence of few adjacent particles, which is adverse for practical application. Anyhow, it concludes that the diatomite addition could well tailor the porous structure of MFCMs.

### 3.6. Purification of oily wastewater

#### 3.6.1. Effect of diatomite contents

The separation performance of MFCMs for oily wastewater treatment is provided in Fig. 9a. It shows that the permeation flux decreases rapidly at the initial stage due to the obstruction of the pores and the increase of permeation resistance of MFCMs [31,32]. Overall, the evolution process of oily wastewater permeating through MFCMs can be illustrated by Fig. 10. In the beginning, the oil droplets in water are rejected by the conjunct effects of adsorption and size exclusion of MFCMs [33]. When the oil droplets stagnate on the surface of MFCMs at the feeding side, they would transform into a liquid film under the driving force of the pressure difference. Then, the film gradually expands to the entire surface with prolonging the running time, leading to the rapid reduction in permeation flux. When the adsorption of MFCMs is saturated with oil droplets, a dense oily cake layer would be formed on the membrane surface. At this time, the filtration of oily wastewater is mainly dominated by size exclusion, with the continuous growth in the thickness of the cake layer. As the result, the permeation flux is slowly decreased. Finally, permeation flux stabilizes at certain values when the filtration system reaches an equilibrium state.

From the adsorption data (Fig. 9b) of MFCMs in 100 mg L<sup>-1</sup> oily wastewater, the adsorption capacity of CM-15% and CM-25% for oil droplets is quickly saturated by 50 min, whereas that of CM-35% continuously increases until to 120 min. The difference is associated with the contribution of the adsorption property of embedded diatomite [34]. In addition, the adsorption behavior of MFCMs is also influenced by the complex porous structure and the interaction between the carbon matrix and diatomite.

Consequently, it brings about the deviation of a few data points from the trend of permeation profiles of MFCMs.

At steady state of 120–240 min, the oil rejection follows the order of CM-25% > CM-15% > CM-35%, which is just opposite to their average pore size and porosity, with no obvious relevance to the surface wettability (Table 1). This implies that the separation process of this stage is mainly predominated by size exclusion, rather than surface wettability of MFCMs [37,38]. In comparison, the separation performance of the as-prepared MFCMs is more

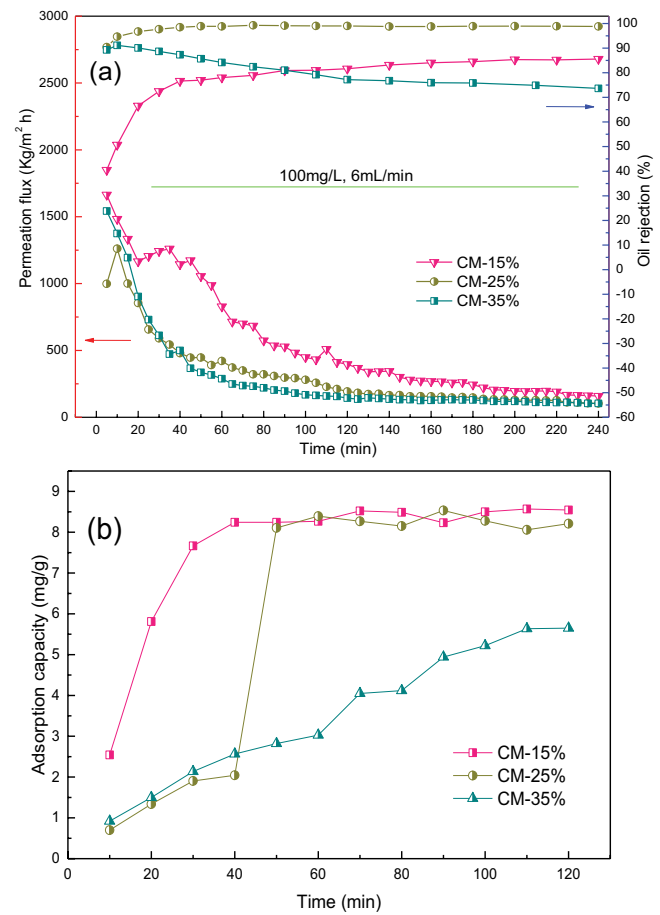


Fig. 9. Effect of diatomite contents on the (a) separation performance and (b) adsorption capacity of MFCMs.

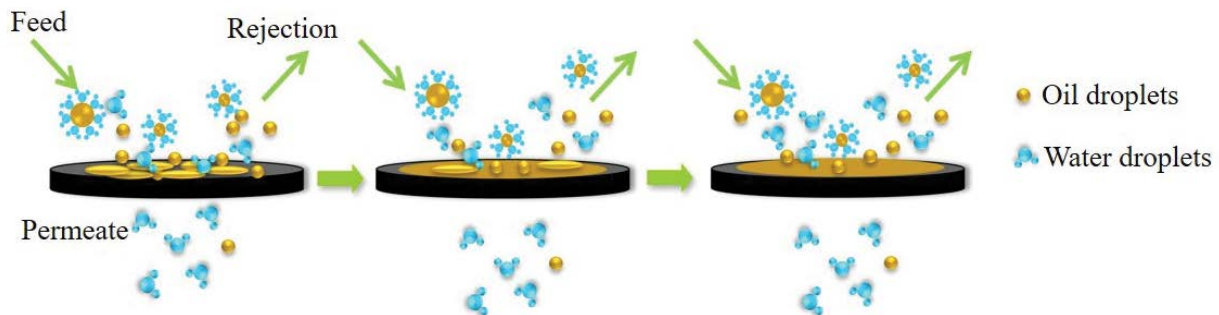


Fig. 10. Evolution process of oily wastewater on the surface of MFCMs.

attractive than some other membrane materials reported in literature (Table 2) [31,35,36]. Additionally, the present oil rejection is also obviously better than our previous work without noticeable loss in permeation flux [23]. The probable reason lies in the modification of remarkably high amount of diatomite. It also shows that the single-stage filtration used in this work is effective for purification of oily wastewater. Moreover, this protocol takes the advantages of more straightforward and cost-effective in operation. In conclusion, CM-25% was selected for further investigation in this study.

### 3.6.2. Effect of feeding oil concentration

Fig. 11 presents the permeation variation of CM-25% at 240 min as the function of feeding oil concentration at a feeding flux of 6 mL min<sup>-1</sup>. As the feeding concentration increases, the permeation flux exhibits a decreasing trend, together with the oil rejection first increasing then decreasing. Under this circumstance, oil beads are more

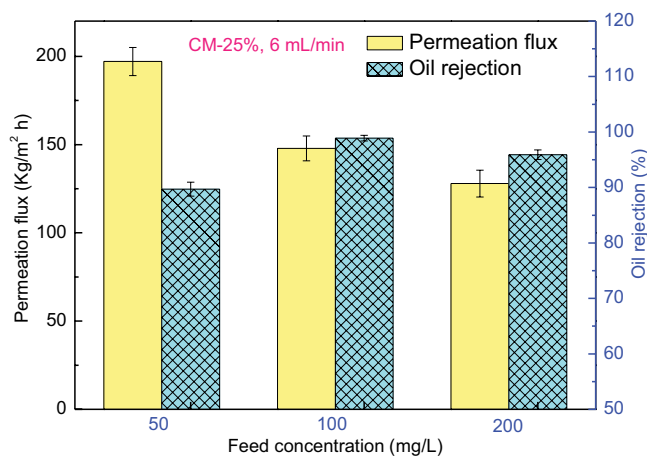


Fig. 11. Effect of feeding concentration on the separation efficiency of oily wastewater.

Table 2

Comparison of the separation performance of various membranes for oily wastewater

References	Membrane samples	Permeation flux	Oil rejection
This work	CM-25%	147.86 kg m <sup>-2</sup> h <sup>-1</sup>	98.9%
Our previous work [23]	CM-15%	175.27 kg m <sup>-2</sup> h <sup>-1</sup>	97.8%
Zhu et al. [31]	Mullite-titania composite membranes	37.5 L m <sup>-2</sup> h <sup>-1</sup>	97%
Yi et al. [35]	CNT-PVA composite membranes	99 L m <sup>-2</sup> h <sup>-1</sup>	88%
Emani et al. [36]	Ceramic membranes	8 × 10 <sup>-6</sup> m <sup>3</sup> m <sup>-2</sup> s <sup>-1</sup>	97.9%

Table 3

Oil concentrations in penetrating fluid by a single filtration stage of CM-25%

Feeding oil concentration (mg L <sup>-1</sup> )	Oil rejection (%)	Concentration at penetration liquid (mg L <sup>-1</sup> )
50	88.30	5.85
100	98.84	1.16
200	95.80	8.40

prone to deposition on the membrane surface or in the pores, resulting into the evolution of a thicker oily cake layer. Consequently, the enhanced permeation resistance depresses the permeation flux.

On the contrary, it needs a longer time for the full formation of a cake layer on MFCMs surface when the feeding concentration is smaller. In this situation, MFCMs are insufficient for exerting size exclusion, leading to some oil beads being entrained or squeezed through the membrane matrix. As the result, the oil rejection fluctuates with feeding concentration. Nevertheless, all the oil concentration of the penetrating liquid is less than 10 mg L<sup>-1</sup> as listed in Table 3, which are satisfied with the national emission standard [39]. In particular, the concentration of the penetrating liquid for CM-25% is much less than 5 mg L<sup>-1</sup>. The result shows that the present MFCMs are quite attractive for purification of oily wastewater.

### 3.6.3. Effect of feeding flux

Fig. 12 shows that the permeation flux and rejection of the MFCMs first increase then decrease with elevating the feeding flux from 4 to 8 mL min<sup>-1</sup>.

Generally speaking, the feeding flux could influence the separation efficiency by two aspects during steady operation stage. The first is the touching probability of membrane with oil beads in a specified given time, which can affect the oil rejection by promoting or retarding the oil cake formation on the surface of MFCMs. On the other hand, the flowing feed stream can also mitigate the adhesion of oil beads on the surface of MFCMs to a certain degree due to the sweeping effect. As the result, the optimum separation efficiency, 98.9% for oil rejection and 147.86 kg m<sup>-2</sup> h<sup>-1</sup>, is achieved at the feeding flux of 6 mL min<sup>-1</sup>.

### 3.6.4. Effect of post-oxidation treatment

Thermal annealing is an effective way to adjust the microstructure and separation performance by opening up pores and introducing functional groups of membrane

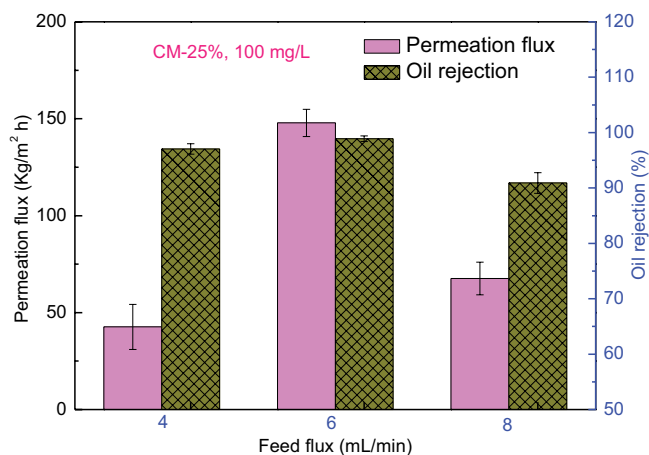


Fig. 12. Effect of feeding flux on the separation efficiency of oily wastewater.

materials [40–42]. In this work, the feasibility of post-oxidation was also attempted for tailoring the microstructure and permeation property of MFCMs.

Fig. 13a shows that the permeation flux is significantly increased after post-oxidation, but the oil rejection decreases from 98.9% to 69.11%. It is certainly ascribed to the enlargement of pore openings and introduction of more oxygen-containing functional groups in MFCMs after oxidative reactions at high temperature and oxidative atmosphere [17]. Anyhow, the result has primarily demonstrated the validity of post-oxidation on the modification of permeation property of MFCMs in spite of requirement of more detailed future works.

As a matter of fact, MFCMs would be inevitably contaminated by the oil beads during the filtration of oily wastewater. On the other hand, the permeation flux of the membrane materials is tightly associated with the resistance to foulants [43]. In this regard, this study further evaluated the anti-fouling ability of the as-prepared MFCMs by four parameters, flux recovery ratio (FRR), reversible fouling ratio ( $R_r$ ), irreversible fouling ratio ( $R_{ir}$ ) and total fouling ratio ( $R_t$ ) [23].

As shown in Fig. 13b, FRR and  $R_r$  significantly increased after post-oxidation, together with the reduction of  $R_{ir}$  and  $R_t$ . The comparative results prove that the utilization of post-oxidation can obviously enhance the anti-fouling ability of MFCMs for oily wastewater. The related work is ongoing in detail by our team, which would be reported in near future.

#### 4. Conclusions

In this study, the oily wastewater was purified by diatomite composite MFCMs through a single-stage filtration. The effects of diatomite contents, oily wastewater concentration and feeding flowrate on the separation efficiency of MFCMs were investigated. As the amount of diatomite increases in MFCMs, the thermal stability of the precursor membranes increases gradually. In the preparation of MFCMs, addition of diatomite with a mass fraction

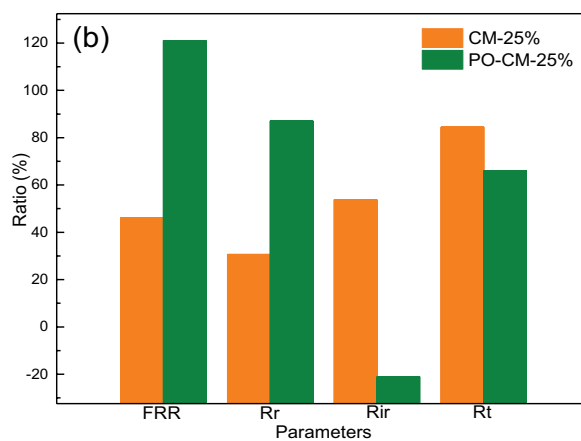
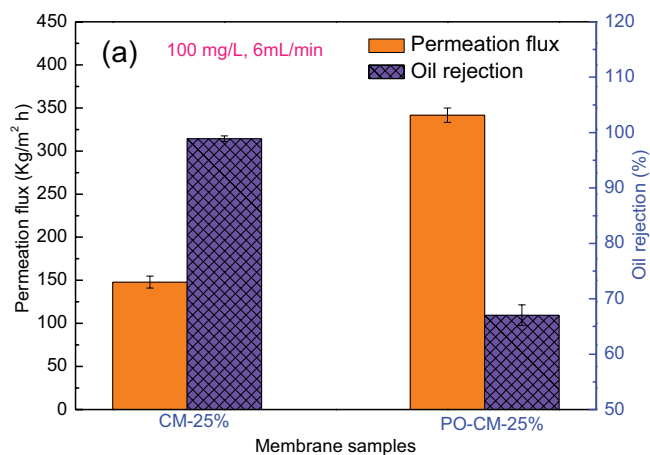


Fig. 13. The effect of post-oxidation on the (a) separation performance and (b) anti-fouling ability of CM-25%.

of 25 wt.% exhibits the highest oil rejection of 98.9% for 100 mg L<sup>-1</sup> oily wastewater, along with the permeation flux of 147.86 kg m<sup>-2</sup> h<sup>-1</sup>, at a feeding flow of 6 mL min<sup>-1</sup>. In addition, the adoption of post-oxidation could greatly improve the permeation flux and anti-fouling property of MFCMs.

#### Acknowledgements

This work was financially supported by the National Natural Science Foundation of China (Nos. 21676044, 21476034), the Liaoning BaiQianWan Talents Program (No. 2018921046), the Fundamental Research Funds for the Central Universities (No. DUT 2018TB02), the Scientific Research Project of Liaoning Provincial Department of Education (No. 2020002), and the Shenyang Youth Science and Technology Project (No. RC200325).

#### References

- [1] U.B. Gunatilake, J. Bandara, Fabrication of highly hydrophilic filter using natural and hydrothermally treated mica nanoparticles for efficient waste oil-water separation, *J. Environ. Manage.*, 191 (2017) 96–104.
- [2] B. Xue, J.G. Deng, J.H. Zhang, Multiporous open-cell poly(vinyl formal) foams for sound absorption, *RSC Adv.*, 6 (2016) 7653–7660.

- [3] N.S. Prasad, S. Moulik, S. Bohra, K.Y. Rani, S. Sridhar, Solvent resistant chitosan/poly(ether-*block*-amide) composite membranes for pervaporation of *n*-methyl-2-pyrrolidone/water mixtures, *Carbohydr. Polym.*, 136 (2016) 1170–1181.
- [4] L. Liu, W. Qiu, E.S. Sanders, C. Ma, W.J. Koros, Post-combustion carbon dioxide capture via 6FDA/BPDA-DAM hollow fiber membranes at sub-ambient temperatures, *J. Membr. Sci.*, 510 (2016) 447–454.
- [5] C.C. Ye, F.Y. Zhao, J.K. Wu, X.D. Weng, P.Y. Zheng, Y.F. Mi, Q.F. An, C.J. Gao, Sulfated polyelectrolyte complex nanoparticles structured nanofiltration membrane for dye desalination, *Chem. Eng. J.*, 307 (2017) 526–536.
- [6] R. Xu, L. Zou, P. Lin, Q. Zhang, J. Zhong, Pervaporative desulfurization of model gasoline using PDMS/BTESE-derived organosilica hybrid membranes, *Fuel Process. Technol.*, 154 (2016) 188–196.
- [7] S. Wang, Y. Wu, N. Zhang, G. He, Q. Xin, X. Wu, H. Wu, X. Cao, M.D. Guiver, Z. Jiang, A highly permeable graphene oxide membrane with fast and selective transport nanochannels for efficient carbon capture, *Energy Environ. Sci.*, 9 (2016) 3107–3112.
- [8] S. Badalov, C.J. Arnusch, Ink-jet printing assisted fabrication of thin film composite membranes, *J. Membr. Sci.*, 515 (2016) 79–85.
- [9] E. Mosayebi, S. Azizian, B.J. Cha, T.G. Woo, Y.D. Kim, Fabrication of highly hydrophobic sand@soot with core-shell structure and large-scale production possibility for oil/water separation, *J. Phys. Chem. Solids*, 150 (2021) 109815, doi: 10.1016/j.jpcs.2020.109815.
- [10] J. Zhang, Q. Xue, X. Pan, Y. Jin, W. Lu, D. Ding, Q. Guo, Graphene oxide/polyacrylonitrile fiber hierarchical-structured membrane for ultra-fast microfiltration of oil-water emulsion, *Chem. Eng. J.*, 307 (2017) 643–649.
- [11] K. Karakulski, M. Gryta, The application of ultrafiltration for treatment of ships generated oily wastewater, *Chem. Pap.*, 71 (2017) 1165–1173.
- [12] X. Zhu, A. Dudchenko, X. Gu, D. Jassby, Surfactant-stabilized oil separation from water using ultrafiltration and nanofiltration, *J. Membr. Sci.*, 529 (2017) 159–169.
- [13] W. Falath, A. Sabir, K.I. Jacob, Highly improved reverse osmosis performance of novel PVA/DGEBA cross-linked membranes by incorporation of Pluronic F-127 and MWCNTs for water desalination, *Desalination*, 397 (2016) 53–66.
- [14] B.S. Al-anzi, O.C. Siang, Recent developments of carbon based nanomaterials and membranes for oily wastewater treatment, *RSC Adv.*, 7 (2017) 20981–20994.
- [15] H. Zhang, Y. Shen, M. Li, G. Zhu, H. Feng, J. Li, Egg shell powders-coated membrane for surfactant-stabilized crude oil-in-water emulsions efficient separation, *ACS Sustainable Chem. Eng.*, 7 (2019) 10880–10887.
- [16] Y. Wu, X. Zhang, S. Liu, B. Zhang, Y. Lu, T. Wang, Preparation and applications of microfiltration carbon membranes for the purification of oily wastewater, *Sep. Sci. Technol.*, 51 (2016) 1872–1880.
- [17] C. Song, T. Wang, J. Qiu, Y. Cao, T. Cai, Effects of carbonization conditions on the properties of coal-based microfiltration carbon membranes, *J. Porous Mater.*, 15 (2008) 1–6.
- [18] C. Li, C. Song, P. Tao, M. Sun, Z. Pan, T. Wang, M. Shao, Enhanced separation performance of coal-based carbon membranes coupled with an electric field for oily wastewater treatment, *Sep. Purif. Technol.*, 168 (2016) 47–56.
- [19] Y. Pan, W. Wang, T. Wang, P. Yao, Fabrication of carbon membrane and microfiltration of oil-in-water emulsion: an investigation on fouling mechanisms, *Sep. Purif. Technol.*, 57 (2007) 388–393.
- [20] L. Du, X. Quan, X. Fan, S. Chen, H. Yu, Electro-responsive carbon membranes with reversible superhydrophobicity/superhydrophilicity switch for efficient oil/water separation, *Sep. Purif. Technol.*, 210 (2019) 891–899.
- [21] M.E. Sayed, M. Ramzi, R. Hosny, M. Fathy, T.A. Moghny, Breakthrough curves of oil adsorption on novel amorphous carbon thin film, *Water Sci. Technol.*, 73 (2016) 2361–2369.
- [22] I. Derbel, R.B. Amar, Preparation of new tubular carbon ultrafiltration membrane for oily wastewater treatment by air gap membrane distillation, *Desal. Water Treat.*, 124 (2018) 21–29.
- [23] X. Zhang, B. Zhang, Y. Wu, T. Wang, J. Qiu, Preparation and characterization of a diatomite hybrid microfiltration carbon membrane for oily wastewater treatment, *J. Taiwan Inst. Chem. Eng.*, 89 (2018) 39–48.
- [24] K. Venkataraman, W.T. Choate, E.R. Torre, R.D. Husung, H.R. Batchu, Characterization studies of ceramic membranes. A novel technique using a Coulter® porometer, *J. Membr. Sci.*, 39 (1988) 259–271.
- [25] J. Yun, L. Chen, X. Zhang, H. Zhao, Z. Wen, C. Zhang, The effects of silicon and ferrocene on the char formation of modified novolac resin with high char yield, *Polym. Degrad. Stab.*, 139 (2017) 97–106.
- [26] B. Zhang, Z. Yu, Y. An, Y. Wu, Y. Shi, Z. Liu, T. Wang, Preparation and characterisation of large sized ordered mesoporous carbon film from resorcinol/formaldehyde by basic catalysts, *Mater. Res. Innovations*, 18 (2014) 294–299.
- [27] X. Zhang, B. Zhang, Y. Wu, D. Wang, T. Wang, Facile preparation of ODPA-ODA type polyetherimide-based carbon membranes by chemical crosslinking, *J. Appl. Polym. Sci.*, 134 (2017) 44889, doi: 10.1002/app.44889.
- [28] J. Yin, J. Zhou, Novel polyethersulfone hybrid ultrafiltration membrane prepared with SiO<sub>2</sub>-g-(PDMAEMA-co-PDMAPS) and its antifouling performances in oil-in-water emulsion application, *Desalination*, 365 (2015) 46–56.
- [29] X. Li, C. Bian, W. Chen, J. He, Z. Wang, N. Xu, G. Xue, Polyaniline on surface modification of diatomite: a novel way to obtain conducting diatomite fillers, *Appl. Surf. Sci.*, 207 (2003) 378–383.
- [30] H.J. Yeom, S.C. Kim, Y.W. Kim, I.H. Song, Processing of alumina-coated clay-diatomite composite membranes for oily wastewater treatment, *Ceram. Int.*, 42 (2016) 5024–5035.
- [31] L. Zhu, M. Chen, Y. Dong, C.Y. Tang, A. Huang, L. Li, A low-cost mullite-titania composite ceramic hollow fiber microfiltration membrane for highly efficient separation of oil-in-water emulsion, *Water Res.*, 90 (2016) 277–285.
- [32] B. Chakrabarty, A.K. Ghoshal, M.K. Purkait, Cross-flow ultrafiltration of stable oil-in-water emulsion using polysulfone membranes, *Chem. Eng. J.*, 165 (2010) 447–456.
- [33] N. Baig, F.I. Alghunaimi, H.S. Dossary, T.A. Saleh, Superhydrophobic and superoleophilic carbon nanofiber grafted polyurethane for oil-water separation, *Process Saf. Environ.*, 123 (2019) 327–334.
- [34] M.A.M. Khraisheh, Y.S. Al-degs, W.A.M. McMinn, Remediation of wastewater containing heavy metals using raw and modified diatomite, *Chem. Eng. J.*, 99 (2004) 177–184.
- [35] G. Yi, S. Chen, X. Quan, G. Wei, X. Fan, H. Yu, Enhanced separation performance of carbon nanotube-polyvinyl alcohol composite membranes for emulsified oily wastewater treatment under electrical assistance, *Sep. Purif. Technol.*, 197 (2018) 107–115.
- [36] S. Emani, R. Uppaluri, M.K. Purkait, Microfiltration of oil-water emulsions using low cost ceramic membranes prepared with the uniaxial dry compaction method, *Ceram. Int.*, 40 (2014) 1155–1164.
- [37] B. Das, B. Chakrabarty, P. Barkakati, Separation of oil from oily wastewater using low cost ceramic membrane, *Korean J. Chem. Eng.*, 34 (2017) 2559–2569.
- [38] G. Shi, Y. Shen, P. Mu, Q. Wang, Y. Yang, S. Ma, J. Li, Effective separation of surfactant-stabilized crude oil-in-water emulsions by using waste brick powder-coated membranes under corrosive conditions, *Green Chem.*, 22 (2020) 1345–1352.
- [39] M. Abbasi, R.S. Mohammad, A. Salahi, B. Mirza, Modeling of membrane fouling and flux decline in microfiltration of oily wastewater using ceramic membranes, *Chem. Eng. Commun.*, 199 (2012) 78–93.
- [40] P. Castejón, D. Arencón, M. Antunes, V. Realinho, J.I. Velasco, A.B. Martínez, Porous membranes based on polypropylene-ethylene copolymers. Influence of temperature on extrusion, annealing and uniaxial strain stages, *Polymers*, 10 (2018) 10080854, doi: 10.3390/polym10080854.

- [41] Z. Rui, J.B. James, Y.S. Lin, Highly CO<sub>2</sub> perm-selective metal-organic framework membranes through CO<sub>2</sub> annealing post-treatment, *J. Membr. Sci.*, 555 (2018) 97–104.
- [42] C. Yin, Z. Wang, Y. Luo, J. Li, Y. Zhou, X. Zhang, H. Zhang, P. Fang, C. He, Thermal annealing on free volumes, crystallinity and proton conductivity of Nafion membranes, *J. Phys. Chem. Solids*, 120 (2018) 71–78.
- [43] L.T. Choong, Y.M. Lin, G.C. Rutledge, Separation of oil-in-water emulsions using electrospun fiber membranes and modeling of the fouling mechanism, *J. Membr. Sci.*, 486 (2015) 229–238.